ACS APPLIED MATERIALS & INTERFACES

Research Article

www.acsami.org

Retardation Mechanism of Ultrathin Al_2O_3 Interlayer on Y_2O_3 Passivated Gallium Nitride Surface

Hock Jin Quah and Kuan Yew Cheong*

Electronic Materials Research Group, School of Materials & Mineral Resources Engineering, Universiti Sains Malaysia, Engineering Campus, Nibong Tebal, Seberang Perai Selatan, Pulau Pinang 14300, Malaysia

ABSTRACT: A systematic investigation was carried out by incorporating an ultrathin aluminum oxide (Al_2O_3) as an interlayer between yttrium oxide (Y_2O_3) passivation layer and GaN substrate. The sandwiched samples were then subjected to postdeposition annealing in oxygen ambient from 400 to 800 °C. The Al_2O_3 interlayer was discovered to play a significant role in slowing down inward diffusion of oxygen through the Y_2O_3 passivation layer as well as in impeding outward diffusion of Ga^{3+} and N^{3-} from the decomposed GaN surface. These beneficial effects have suppressed subsequent formation of interfacial layer. A mechanism in association with the function of Al_2O_3 as an interlayer was suggested and discussed. The mechanism was explicitly described on the basis of the obtained results from X-ray diffraction, X-ray photoelectron spectroscopy, energy-filtered transmission electron microscopy (TEM), high resolution TEM, and electron energy loss spectroscopy line scan. A correlation between the proposed mechanism and metal-oxide-semiconductor characteristics of Y_2O_3/Al_2O_3/GaN structure has been proposed.

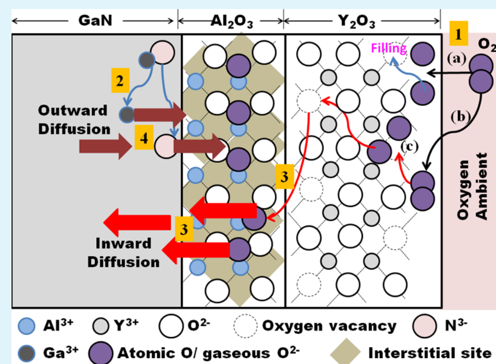

KEYWORDS: *gallium nitride, yttrium oxide, aluminum oxide, mechanism, diffusion*

1. INTRODUCTION

Keeping in track with the development of gallium nitride (GaN)-based metal-oxide-semiconductor (MOS) devices for high power and high temperature applications, which strive to solve the ever-increasing demand of global energy consumption, challenges pertaining to the implementation of a high quality passivation layer on GaN substrate surface are inexorable.[1−3] Numerous low-dielectric constant (k) and high-k materials, which include SiO_2,[4,5] SiN_xO_y,[6] Al_2O_3,[2,3,7,8] HfO_2,[1,9] Sc_2O_3,[10] $Ga_2O_3(Gd_2O_3)$,[11] Gd_2O_3,[12] Y_2O_3,[13,14] Ga_2O_3,[15,16] $MgTiO_3$,[17] Ta_2O_5,[18] MgO,[19] MgScO,[19] CeO_2,[20,21] and HfAlO,[22] have been researched. Of these materials, the attention devoted to the utilization of Y_2O_3 as the passivation layer in GaN-based MOS devices remains meager. Apart from the fascinating properties of Y_2O_3, which are composed of high-k value (k = 12−18), large bandgap (∼5.5 eV), and large conduction band offset (∼1.97 eV),[13,14] Y_2O_3 has been designated for its cubic bixbyite structure with two corners of the cube not being occupied by oxygen ions.[23−25] Having this bixbyite structure, Y_2O_3 is regarded as a high-k material with oxygen vacancies.[13,14,23−25] The presence of oxygen vacancies in the Y_2O_3 layer is deemed as the impediment that may degrade the interfacial quality between the Y_2O_3 layer and substrate contributing to the deterioration of MOS characteristics. Thus, postdeposition annealing (PDA) in oxygen ambient, which has been reported for Y_2O_3 layer deposited on Si and GaN substrates,[14,26] is formulated to trim down the adverse effects of oxygen vacancies.[27] Another effective approach in confronting this shortcoming is through the employment of a stacking passivation layer, which has been proven for its effectiveness in enhancing the MOS characteristics through the inclusion of a thin SiO_2 interlayer at the interface between Y_2O_3 and Si.[28] However, emulation of this constructive approach in GaN-based MOS devices has encountered a limitation, wherein the possession of a relatively low-k value by SiO_2 when compared with GaN will contribute to the premature breakdown of this device.[29]

In the selection of a suitable interlayer to serve the aforementioned purpose, two criteria ought to be taken into consideration. The interlayer has to possess a high-k value to discard the concern of premature breakdown of the device and a low density of oxygen-related defects in the passivation layer to prevent degradation of interfacial quality. Thus far, a swing of direction has been developed toward the integration of high-k α-Al_2O_3 as the interlayer between the Y_2O_3 and GaN. This is owing to the attainment of a high-k value (k = 8−10), a large bandgap (7−9 eV), and a large conduction band offset (∼2.16 eV),[2,30,31] as well as the rhombohedral unit cell of α-Al_2O_3, which favors the formation of oxygen interstitials.[32−34] Therefore, α-Al_2O_3 is also designated as the oxygen interstitial former. This property of α-Al_2O_3 may serve as the helping hand to build a barrier that restricts the passage of oxygen to the surface of GaN substrate. Besides acting as an oxygen interstitial former, another essential function of α-Al_2O_3 is to restrain the

Received: February 21, 2014
Accepted: April 8, 2014
Published: April 8, 2014

 © 2014 American Chemical Society

extent of nitrogen and gallium acquired from the decomposition of GaN (≥400 °C) to diffuse outward[14,35] to the Y_2O_3 layer. Hence, the suppression of interfacial layer (IL) formation could be achieved, and this has been supported by atomic-layer-deposited HfO_2/Al_2O_3 stacking layers on GaN.[9] Although the effectiveness of this interlayer in suppressing the formation of IL has been proven, a detailed mechanism of α-Al_2O_3 in inhibiting the IL formation has not been studied or proposed. Therefore, present work aims to discuss the mechanism via the correlation among chemical, structural, and MOS characteristics for RF-magnetron sputtered Y_2O_3/Al_2O_3 stacking layers on GaN substrate subjected to PDA from 400 to 800 °C in oxygen ambient.

2. RESULTS AND DISCUSSIONS

The function of Al_2O_3 as an interlayer in Y_2O_3/Al_2O_3/GaN samples that have been subjected to different postdeposition annealing (PDA) temperatures (400, 600, and 800 °C) in oxygen (O_2) ambient can be described using a proposed mechanism, comprising four primary steps, as schematized in

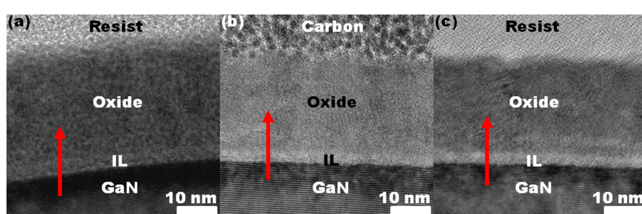

Figure 1. Cross-sectional energy filtered transmission electron microscopy (TEM) images of Y_2O_3/Al_2O_3/GaN structures PDA at (a) 400 °C and (c) 800 °C, as well as high resolution TEM image of Y_2O_3/Al_2O_3/GaN structure PDA at (b) 600 °C. Red arrow indicates the particular depth of interest and direction of electron energy loss spectroscopy line scan.

Figure 2. These steps instigate from (1) adsorption of O_2 molecules into Y_2O_3 layer, (2) decomposition of GaN substrate that happens concurrently with step (1), (3) inward diffusion of atomic and/or molecular oxygen, and (4) outward diffusion of decomposed Ga^{3+} and N^{3-} to Al_2O_3 layer.

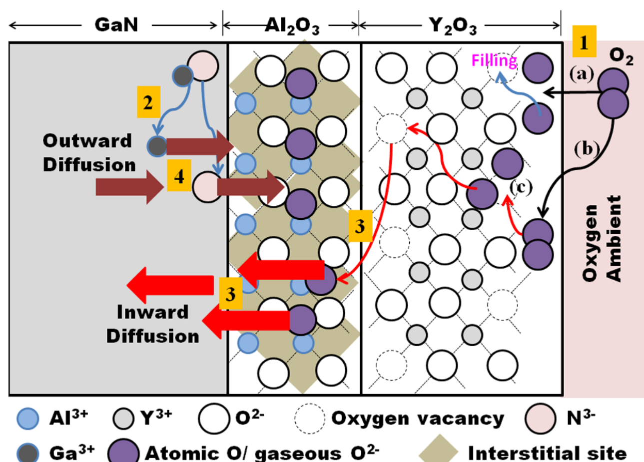

Figure 2. Schematic diagram showing mechanism occurring in Y_2O_3/Al_2O_3/GaN structures PDA at different temperatures (400−800 °C). Labels (a), (b), and (c) represent, respectively, the adsorbed atomic O, molecular O_2, and adsorption of the molecular O_2 on oxygen vacancy site in Y_2O_3.

Initially, O_2 molecules from the ambient are adsorbed on the surface[36] of the Y_2O_3 layer (step 1) during PDA. This surface adsorption process will either form molecular O_2 (step 1b) or atomic O (step 1a). These adsorbed O_2 and/or atomic O will subsequently diffuse into the Y_2O_3 layer. Upon diffusion, the molecular O_2 could possibly adsorb on oxygen vacancy (step 1c) sites in Y_2O_3[37,38] since oxygen vacancy could serve as the adsorption site for O_2 molecules. The presence of oxygen vacancies in Y_2O_3 is due to the attainment of cubic bixybite structure, which is supported by X-ray diffraction (XRD) for the Y_2O_3 (ICDD file no. 00-041-1105) phase oriented in (222) and (400) planes for samples PDA from 400 to 800 °C (Figure 3). In cubic bixbyite Y_2O_3, a Y cation is located in the center of

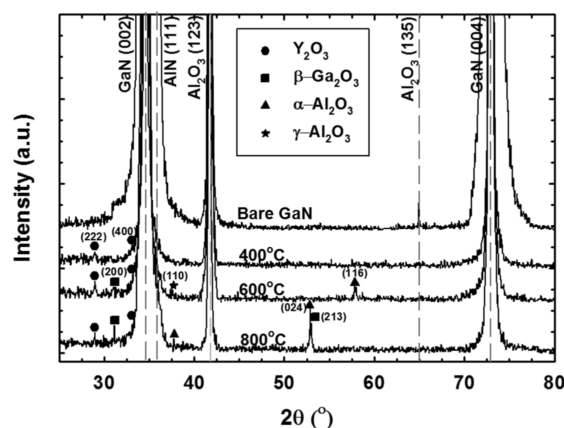

Figure 3. XRD patterns of postdeposition annealed samples and bare GaN substrate.

the cube with six oxygen anions occupying corners of the cube, whereby two remaining oxygen sites are vacant.[24,25,39] Therefore, apart from the surface adsorption, the existence of oxygen vacancies in Y_2O_3 as additional adsorption sites[37] would facilitate the O_2 adsorption process. During the adsorption of O_2 molecule on one oxygen vacancy, a charge transfer from the neighboring lattice oxygen anions (O^{2-}) to the O_2 molecules happens and the O_2 molecules become negatively charged (O_2^{2-}). The electron transfer from O^{2-} will lead to the formation of atomic O while the O_2^{2-} species are then dissociated to monatomic $2O^{2-}$ ions. The adsorption phenomenon from O_2 molecule to monatomic $2O^{2-}$ has been termed as the dissociative adsorption process.[37,40] Three possible scenarios have been suggested for the O_2 adsorption process on oxygen vacancies, as follows:

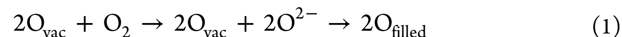

$$2O_{vac} + O_2 \rightarrow 2O_{vac} + 2O^{2-} \rightarrow 2O_{filled} \quad (1)$$

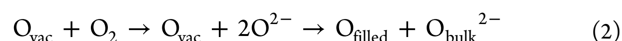

$$O_{vac} + O_2 \rightarrow O_{vac} + 2O^{2-} \rightarrow O_{filled} + O_{bulk}^{2-} \quad (2)$$

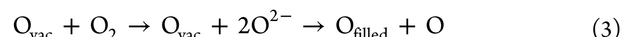

$$O_{vac} + O_2 \rightarrow O_{vac} + 2O^{2-} \rightarrow O_{filled} + O \quad (3)$$

where O_{vac} represents oxygen vacancy, O_{filled} is a filled/occupied vacancy site, O_{bulk}^{2-} is O^{2-} from ambient that diffuses to Y_2O_3 lattice, and O is an atomic O. In scenario (eq 1), the dissociated $2O^{2-}$ ions will fill two oxygen vacancies in Y_2O_3, forming $2O_{filled}$. Scenario (eq 2) differs from scenario (eq 1) since only one oxygen vacancy is being filled/occupied in scenario (eq 2). The other O^{2-} ion (O_{bulk}^{2-}) will reside in Y_2O_3 lattice, and there is a possibility for this ion to transform to atomic O, as

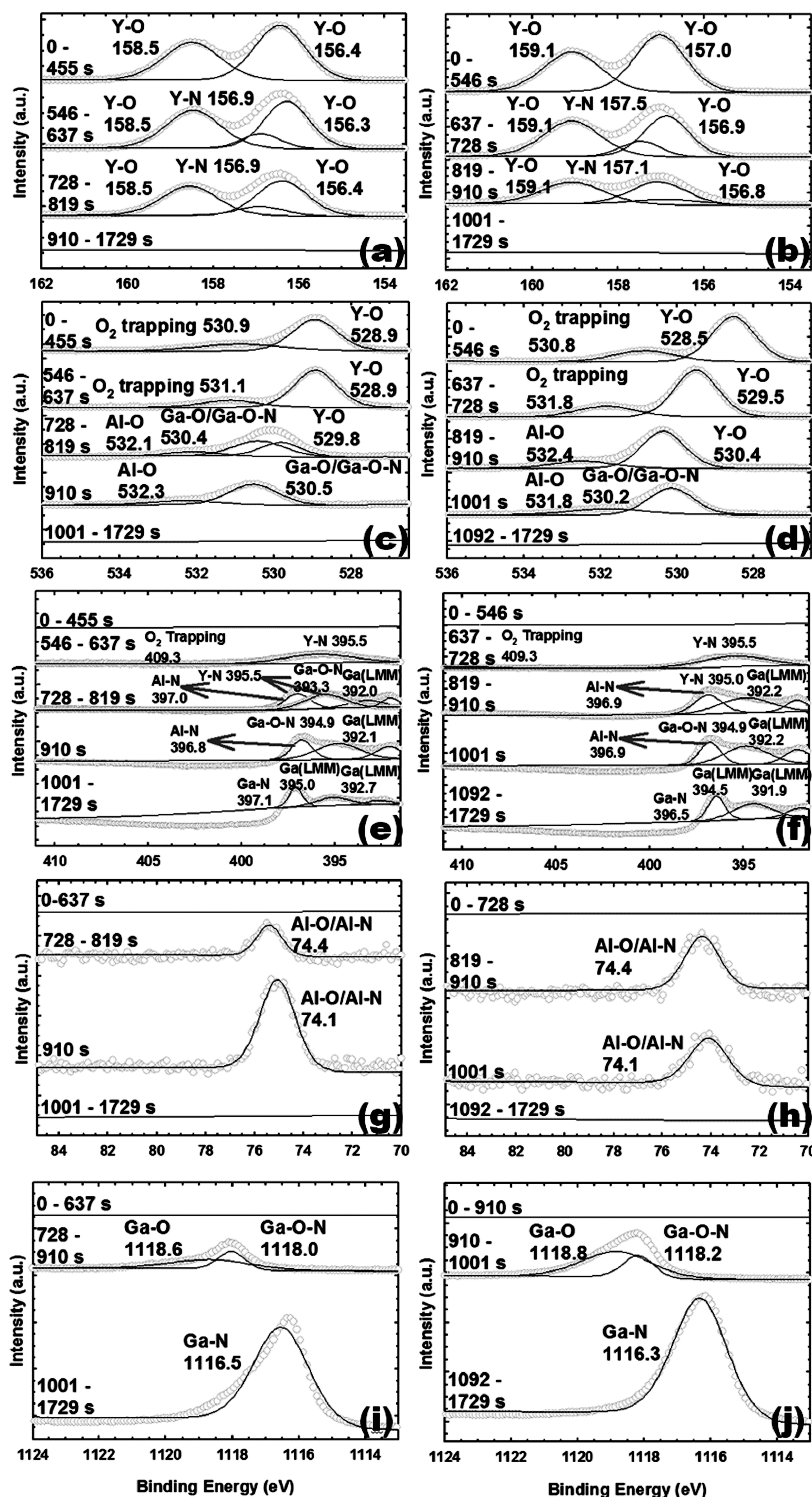

Figure 4. XPS core level spectra of Y 3d, O 1s, N 1s, Al 2p, and Ga 2p for $Y_2O_3/Al_2O_3/GaN$ structures PDA at 800 °C [Y 3d (a), O 1s (c), N 1s (e), Al 2p (g), and Ga 2p (i)] and 400 °C [Y 3d (b), O 1s (d), N 1s (f), Al 2p (h), and Ga 2p (j)].

envisaged in scenario (eq 3). The transformation of O_{bulk}^{2-} to atomic O has contributed to the release of two electrons from the O_{bulk}^{2-}. These two released electrons will be transferred to the inward diffusing O_2 molecules from the ambient. With this, direct transformation of O_2 molecules to O_{bulk}^{2-} may happen without going through the adsorption process. In Y_2O_3, occupancy of the oxygen vacancies by the adsorbed O^{2-} from ambient will perturb charge neutrality. Therefore, charge compensation has to be achieved to recover charge neutrality in Y_2O_3. Nonetheless, oxidation state of Y^{3+} is unchanged since Y^{3+} is not a multivalence cation like Ce^{4+}, which can be changed to Ce^{3+} or vice versa.[41] Alternatively, it is anticipated that the charge neutrality in Y_2O_3 has been compensated by releasing the atomic O, which has been formed after the charge transfer

of lattice O^{2-} to the O_2 molecule. The release of atomic O will reintroduce an oxygen vacancy in Y_2O_3. As a whole, O_2 adsorption process in Y_2O_3 is accompanied by the acquisition of O_{filled}, atomic O, and O_{bulk}^{2-}. These oxygen species (atomic O and O_{bulk}^{2-}) may either diffuse to the Al_2O_3 layer or be trapped in the Y_2O_3 layer. X-ray photoelectron spectroscopy (XPS) core level spectra of O 1s have shown an oxygen trapping related peak at a binding energy of 530.8 and 530.9 eV for samples PDA at 400 and 800 °C, respectively (Figure 4c,d). The detection of this peak symbolizes the presence of oxygen species that are trapped in the Y_2O_3 layer. In addition, some of the oxygen species will diffuse to Al_2O_3 interlayer at the expense of oxygen vacancies in Y_2O_3 as a diffusion channel. The oxygen species will migrate from one oxygen vacancy to another through a hopping mechanism,[42] in which this oxygen migration process will facilitate oxygen mobility[43] diffusing through the Y_2O_3 layer.

Apart from the adsorption of O_2 molecules in Y_2O_3 layer (step 1), decomposition of GaN substrate (step 2) happens simultaneously with step (1) during PDA. This could be supported on the basis of the detection of N element from region 5 to 2 and Ga element from region 5 to 4 using XPS depth profiling analysis (Figure 5) and electron energy loss spectroscopy (EELS) line scan (Figure 6) for the PDA samples. The detection of Ga element by XPS depth profiling analysis (Figure 5) and EELS line scan (Figure 6) is extended to region 3 when PDA temperature is increased beyond 600 °C. This signifies that outward diffusion of gaseous N^{3-} and Ga^{3+} from region 5 (GaN substrate) to the layers of Al_2O_3 and/or Y_2O_3 happens due to the decomposition of GaN. The decomposition of GaN has been reported to initiate at 400 °C.[14,35] Despite that, it is observed from both XPS depth profile (Figure 5) and EELS line scan (Figure 6) that the N profile is extended from region 5 to 2, which is farther away from the Ga profile. The reason contributing to this observation is due to a slower diffusion of Ga^{3+} when compared with N^{3-}, wherein decomposition of GaN will form liquid Ga^{3+} prior to transformation to gaseous Ga^{3+}. As the gaseous Ga^{3+} and N^{3-} are diffusing outward, an interaction happens between the Ga^{3+} and N^{3-} with oxygen species that have diffused inward through the Y_2O_3 layer. This interaction would lead to the formation of interfacial layer (IL) comprising Ga−O and Ga−O−N compounds, which have been corroborated by the acquired XRD (Figure 3) and XPS core level spectra (Figure 4) results. XRD analysis has successfully detected the presence of β-Ga_2O_3 (ICDD file no. 01-074-1776) phase oriented in the (200) plane in samples PDA at temperatures beyond 600 °C. An additional β-Ga_2O_3 phase oriented in (213) plane is detected when the sample is PDA at 800 °C. On the other hand, XPS core level spectra of Ga 2p, O 1s, and N 1s have suggested the presence of Ga−O and Ga−O−N compounds in samples PDA at 400 and 800 °C (Figure 4). On the basis of the findings from XRD and XPS, it is conclusive to say that the IL is composed of Ga−O and Ga−O−N compounds for samples PDA from 400 to 800 °C. However, the Ga−O compound present in the IL of the sample PDA at 400 °C is in amorphous phase due to the nonexistence of β-Ga_2O_3 peak from XRD characterization (Figure 3).

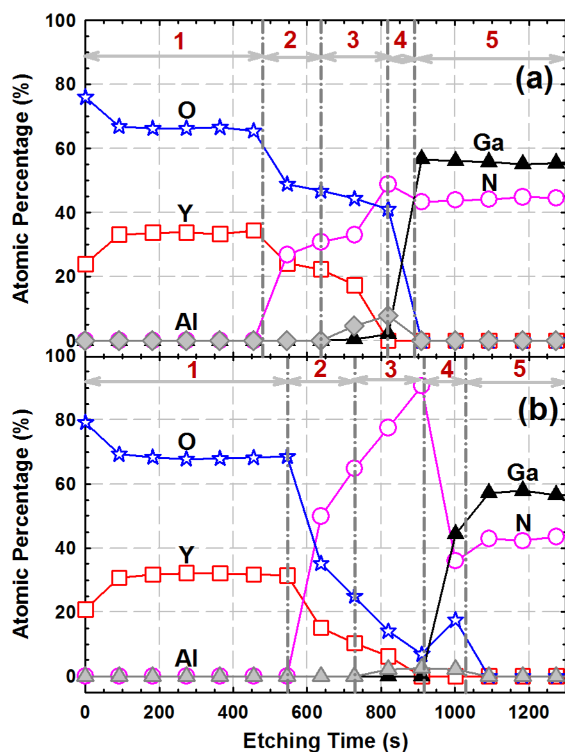

Figure 5. XPS depth profiles of samples postdeposition annealed at (a) 800 and (b) 400 °C.

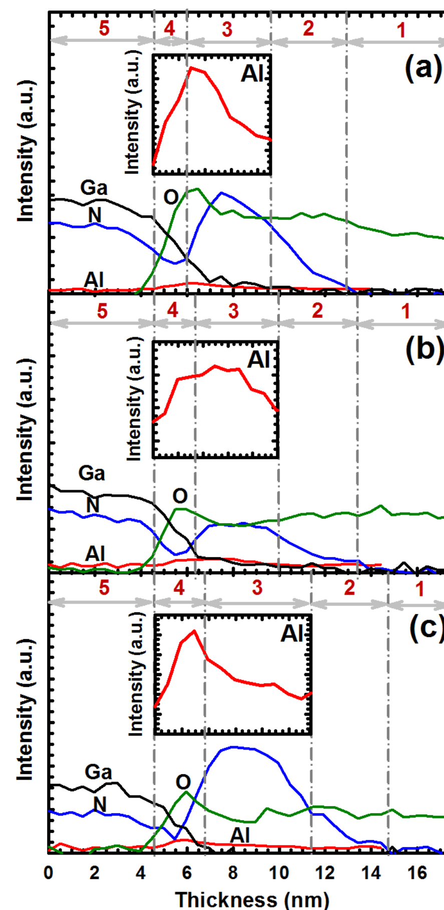

Figure 6. Electron energy loss spectroscopy line scan profiles of Al, O, Ga, and N for $Y_2O_3/Al_2O_3/GaN$ structures PDA at (a) 800 °C, (b) 600 °C, and (c) 400 °C.

A comparison between $Y_2O_3/Al_2O_3/GaN$ and Y_2O_3/GaN structures[14] subjected to PDA at 400 °C in O_2 ambient

dx.doi.org/10.1021/am501075s | ACS Appl. Mater. Interfaces 2014, 6, 7797−7805

ascertains that Al_2O_3 has succeeded in restraining the outward diffusion of Ga^{3+} and N^{3-} to the Y_2O_3 layer. This has been proven on the basis of XPS depth profiling analysis, which shows that the outward diffusing N^{3-} is extended to the entire region of Y_2O_3 (total sputtering time of 1500 s) for Y_2O_3/GaN structure[14] while this N^{3-} is only able to diffuse until a particular region of Y_2O_3 (region 2; total sputtering time of 545 s) for Y_2O_3/Al_2O_3/GaN structure (Figure 5). Besides, the total sputtering time for outward diffusion of Ga^{3+} (115 s) in Y_2O_3/Al_2O_3/GaN structure (Figure 5) is lower than that of Y_2O_3/GaN structure (660 s).[14] Another beneficial effect of Al_2O_3 as an interlayer in the Y_2O_3/Al_2O_3/GaN structure is the effectiveness of Al_2O_3 to restrict oxygen species from diffusing inward to the GaN surface. This is due to the crystal structure of Al_2O_3 that is able to form oxygen interstitial network, wherein this Al_2O_3 is known as an oxygen interstitial former.[32−34] In order to distinguish the peaks related to sapphire substrate from the Al_2O_3 interlayer deposited on GaN substrate, XRD pattern of a bare GaN sample has been included for comparison with the investigated PDA samples (Figure 3). It is perceived that the GaN (ICDD file no. 00-050-0792), Al_2O_3 (ICDD file no. 01-088-0107), and AlN (ICDD file no. 01-087-1053) phases have been detected in all of the investigated samples (Figure 3). The Al_2O_3 (ICDD file no. 01-088-0107) peaks oriented in (123) and (135) planes are referred to as the sapphire substrate. The detection of AlN phase oriented in (111) plane is due to the growth of AlN as a buffer layer on sapphire substrate to reduce the lattice mismatch (16%) between the GaN epitaxial layer and sapphire substrates. In this work, rhombohedral phase of α-Al_2O_3 (ICDD file no. 01-074-0323) oriented in (116) plane and cubic phase of γ-Al_2O_3 (ICDD file no. 00-010-0425) oriented in (311) plane have been detected using XRD characterization for a sample PDA at 600 °C (Figure 3). This indicates that a mixture of α-Al_2O_3 and γ-Al_2O_3 phases is formed for a sample PDA at 600 °C. This is in agreement with previously reported results of Al_2O_3 layer deposited using pulsed magnetron sputtering, wherein γ-Al_2O_3 phase started to form at 480 °C while a mixture of α-Al_2O_3 and γ-Al_2O_3 phases was formed at 690 °C.[44] Further increasing of the PDA temperature to 800 °C, the peaks related to α-Al_2O_3 phase oriented in (110) and (024) planes are detected. The detection of α-Al_2O_3 phase at this temperature (800 °C), which is higher than the reported pulsed magnetron sputtered Al_2O_3 layer at 760 °C[44] further supported the presence of only α-Al_2O_3 phase at 800 °C in the present work. The absence of XRD peaks related to α-Al_2O_3 and γ-Al_2O_3 in a sample PDA at 400 °C suggested that the Al_2O_3 interlayer is in amorphous phase or nonexistence of Al_2O_3 interlayer in this sample. Thus, further investigation using XPS core level spectra of Al 2p and O 1s as well as EELS line scan has revealed the existence of Al−O compound (Figure 4) and the presence of Al and O profiles in region 3 and 4 (Figure 6), respectively. This denotes the existence of Al_2O_3 in amorphous phase for a sample PDA at 400 °C. As a whole, the Al_2O_3 interlayer is transformed from amorphous to polycrystalline phase when PDA is carried out beyond 600 °C.

In rhombohedral phase of α-Al_2O_3, oxygen layers are arranged as close-packed stack with Al coordinating in the octahedral interstitial position.[34] In each layer, one-third of the octahedral interstitial site remains vacant.[34] When oxygen species are migrating from Y_2O_3 layer to α-Al_2O_3 interlayer during PDA (step 3), the oxygen species tend to settle at the interstitial sites and become the interstitial oxygen atoms. It has been reported in previous literature that the interstitial oxygen atoms are coordinated with Al sites favorably in a split interstitial configuration.[34] Therefore, it was observed from the EELS line scan that the profile of O at region 3 and 4 (Figure 6) mimics the profile of Al at similar regions (inset of Figure 6) for a Y_2O_3/Al_2O_3/GaN structure PDA from 400 to 800 °C. It is believed that the formation of interstitial oxygen in α-Al_2O_3 has substantially slowed down the diffusion of oxygen species to the GaN surface leading to the formation of a thinner IL for Y_2O_3/Al_2O_3/GaN structure when compared with Y_2O_3/GaN structure.[29] This could be supported on the basis of the cross-sectional energy filtered transmission electron microscopy (EFTEM) images for a Y_2O_3/Al_2O_3/GaN structure PDA at 400 °C (Figure 1a) and 800 °C (Figure 1c) as well as a high resolution transmission electron microscopy (HRTEM) image for a Y_2O_3/Al_2O_3/GaN structure PDA at 600 °C (Figure 1b), in which the IL thicknesses in the range of 1.8 to 2.4 nm have been acquired. It is deemed that the Y_2O_3/Al_2O_3/GaN structure has achieved its intention of suppressing the formation of the IL as the thickness of the IL for Y_2O_3/GaN structure subjected to PDA from 400 to 800 °C in argon ambient, which is known as an oxygen poor condition, is approximately 2.6−13.5 nm.[29]

In spite of the slowdown process of oxygen diffusion, the α-Al_2O_3 interlayer can also serve as a layer to accumulate the outward diffusing Ga^{3+} and N^{3-}. The ability of the α-Al_2O_3 interlayer to accumulate N^{3-} and Ga^{3+} can be explained as follows. In the event of GaN decomposition, N^{3-} and Ga^{3+} will diffuse outward (step 4) from the GaN surface (region 5; as shown in Figures 5 and 6) to react with the inward diffusing oxygen species to form IL comprising Ga−O and Ga−O−N compounds. Since liquid Ga^{3+} and gaseous N^{3-} are formed at the initial stage of GaN decomposition, the IL formed is deficit of Ga^{3+} but rich in N^{3-} and oxygen species leading to the occurrence of charge imbalance in the IL. As a result, there is a tendency for the neighboring α-Al_2O_3 interlayer to transfer its Al^{3+} to the IL for charge compensation. With this, IL consisting of Al−Ga−O−N is formed, as observed in region 4 in XPS depth profiling (Figure 5) and EELS line scan (Figure 6) for all of the investigated samples. In order to determine the compound present in the region of the IL for all of the investigated samples, XPS core level spectra of Al 2p, Ga 2p, O 1s, and N 1s have been carried out and Al−O, Al−N, Ga−O, and Ga−O−N compounds[45−47] have been detected in this region (Figure 4).

When Al^{3+} is diffusing from the α-Al_2O_3 interlayer (region 3) to the IL (region 4), the interstitial oxygen coordinated to the Al^{3+} will also diffuse concurrently to the IL. The inward diffusion of Al^{3+} and interstitial oxygen to the IL (region 4) has contributed to charge imbalance in the α-Al_2O_3 interlayer (region 3). Therefore, outward diffusing N^{3-} from the GaN surface (region 5) will be captured by α-Al_2O_3 interlayer (region 3) to achieve charge neutrality. It is anticipated that the α-Al_2O_3 interlayer has a preference of capturing N^{3-} due to the "+3" charge carried by Al^{3+} and "−3" charge carried by N^{3-}. This can be observed in EELS line scan for N profile, which accumulates mainly in region 3 (Figure 6) for the Y_2O_3/Al_2O_3/GaN samples PDA from 400 to 800 °C. This observation is in agreement with the XPS depth profiling of N profile for Y_2O_3/Al_2O_3/GaN samples PDA at 400 and 800 °C (Figure 5). Besides, the outward diffusion of N^{3-} to α-Al_2O_3 interlayer is more rapid than that of Ga^{3+} due to the requirement of transforming the liquid Ga^{3+} to gaseous Ga^{3+}. Hence, the α-

Al_2O_3 interlayer is in excess of negative charges, and charge compensation is being achieved through the diffusion of Y^{3+} and/or Ga^{3+} to the α-Al_2O_3 interlayer (region 3). It is designated that only Y^{3+} is diffusing to the α-Al_2O_3 interlayer (region 3) to achieve charge neutrality due to the nondetection of Ga profile in region 3 from EELS line scan (Figure 6) and XPS depth profiling analysis (Figure 5) as well as the detection of Y profile in region 3 from XPS depth profiling analysis (Figure 6). Thus, it was determined through XPS depth profiling analysis that region 3 consisted of Y−Al−O−N for a sample PDA at 400 °C (Figure 5). The results obtained from XPS core level spectra of Y 3d, Al 2p, O 1s, and N 1s denote the formation of Y−O, Y−N, Al−O, and Al−N compounds[45,48−51] in region 3 for a sample PDA at 400 °C (Figure 4). When PDA is increased beyond 600 °C, it is believed that the outward diffusion of Ga^{3+} is being enhanced leading to the formation of Y−Al−Ga−O−N in region 3. The diffusion of Ga^{3+} and Y^{3+} to α-Al_2O_3 interlayer (region 3) can be testified on the basis of the detection of Ga profile in region 3 through EELS line scan (Figure 6) and XPS depth profiling analysis (Figure 5) as well as Y profile from XPS depth profiling analysis (Figure 5). It was resolved from XPS core level spectra of Y 3d, Al 2p, O 1s, Ga 2p, and N 1s that Y−O, Y−N, Al−O, Al−N, Ga−O, and Ga−O−N compounds[45−51] are formed in region 3 (Figure 4). Since region 3 has attained charge neutrality through the diffusion of Ga^{3+}, Y^{3+}, N^{3-}, and oxygen species to the α-Al_2O_3 interlayer, the excess of either ions in region 3 will diffuse outward to region 2 and/or inward to region 4. Therefore, it is observed that N^{3-} is diffusing outward to region 2 leading to the formation of Y−O−N as denoted by XPS depth profiling analysis for all of the investigated samples (Figure 5). This region 2 consisted of Y−O and Y−N compounds as well as oxygen trapping[48−51] as indicated by XPS core level spectra of Y 3d, O 1s, and N 1s for all of the investigated samples (Figure 4). It is believed that the detection of oxygen trapping in region 2 is referred to as the $N{\equiv}O_3$[52] due to the detection of oxygen trapping peak in both XPS core level spectra of O 1s and N 1s (Figure 4c−f) while oxygen trapping in region 1 is referred to as the trapping of oxygen species in Y_2O_3 layer since oxygen trapping peak is only being detected by XPS core level spectrum of O 1s (Figure 4c,d).

Although charge neutrality may have been achieved by the outward diffusing Ga^{3+} and N^{3-} and inward diffusing O^{2-} as well as the diffusion of neighboring Al^{3+} or Y^{3+}, not necessarily all the diffusing Ga^{3+}, N^{3-}, and O^{2-} have taken place in the charge compensation. These ions would therefore stay in the oxide layer as unbonded ions in the Y_2O_3/Al_2O_3/GaN structure. It is anticipated that inward diffusing O^{2-} from the O_2 ambient as well as outward diffusing Ga^{3+} and N^{3-} from the GaN decomposition are the major influential considerations in determining the overall dominance of positive or negative charges in the structure. Of these three ions, the interstitial sites of α-Al_2O_3 will be predominantly occupied by the inward diffusing O^{2-} and outward diffusing N^{3-}. The reason contributing to this anticipation is due to a slower outward diffusion of Ga^{3+} than N^{3-} to the α-Al_2O_3 interlayer. Thus, the number of Ga^{3+} occupying the interstitial sites of α-Al_2O_3 is less, and more unbonded Ga^{3+} ions are available in the α-Al_2O_3 interlayer. This may contribute to the dominance of positive charges in Y_2O_3/Al_2O_3/GaN structure, which was supported by measuring the high-frequency (100 kHz) capacitance−voltage (C−V) curves for the GaN-based MOS capacitors with Y_2O_3/Al_2O_3 as the gate stack subjected to different PDA temperatures (Figure 7). Negative flatband voltage shift (ΔV_{FB}) is observed from the C−V curves indicating the presence of positively charged traps in the investigated samples.[29] When PDA temperature is being increased, an increment in the negative ΔV_{FB} signifies the presence of more positively charged traps in the samples. One of the reasons contributing to this observation is due to the enhancement in the decomposition of GaN as a function of PDA temperature, wherein more unbonded Ga^{3+} ions will be residing in the α-Al_2O_3 interlayer. Besides Ga^{3+} ions, the N^{3-} ions formed from the decomposition of GaN are also enhanced at a higher PDA temperature. However, these N^{3-} ions will be bonded to the oxygen species, forming oxygen trapping that is denoted as $N{\equiv}O_3$ (Figure 4c−f) and has been discussed previously. In order to further support the attainment of positive charges in the investigated structures, effective oxide charges (Q_{eff}) have been calculated using following equation:[29]

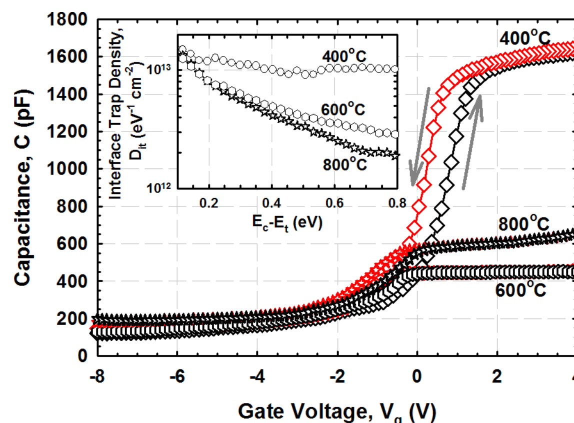

Figure 7. High frequency capacitance−gate voltage (C−V) characteristics of GaN-based MOS capacitors with Y_2O_3/Al_2O_3 gate stack PDA at different temperatures. Inset shows interface trap density obtained for the investigated samples.

$$Q_{eff} = \frac{\Delta V_{FB} C_{ox}}{qA} \tag{4}$$

where ΔV_{FB} is flatband voltage shift, C_{ox} is maximum accumulation capacitance, q is the electronic charge, and A is the capacitor area. The calculated Q_{eff} in the range of (0.53−1.55) × 10^{12} cm^{-2} is obtained for the investigated samples, which is in accordance with the trend of trap density observed from the estimation of traps using ΔV_{FB}. In addition, it is deduced from Q_{eff} calculation that positive traps are the dominating charges in Y_2O_3/Al_2O_3/GaN structure PDA at different temperatures.

The aforementioned discussion has signified that decomposition of GaN substrate will initially form liquid Ga^{3+} and gaseous N^{3-} during PDA (≥400 °C). In order for these Ga^{3+} to diffuse outward, a transformation from liquid Ga^{3+} to gaseous Ga^{3+} is required. Hence, the formation of gaseous Ga^{3+} will become more dominant than liquid Ga^{3+} when PDA temperature is being increased. The presence of liquid Ga^{3+} on the GaN surface is projected to cause degradation in the interface quality of the investigated samples, whereby a sample PDA at a higher temperature will demonstrate a better interface quality. This expectation was reinforced by the estimation of the oxide-GaN interface trap density (D_{it}) of the investigated samples using Terman's method:[53]

$$D_{it} = \frac{C_{ox}d(\Delta V_g)}{qAd(\Phi_s)} \quad (5)$$

where $\Delta V_g = V_g - V_{g(ideal)}$ is the voltage shift of the experimental curve from the ideal curve, V_g is the experimental gate voltage, and Φ_s is the surface potential of GaN at a specific gate voltage. On the basis of the obtained D_{it} value for the investigated samples (inset of Figure 7), it is proclaimed that interface quality of the investigated samples is improved as the PDA temperature is increased. Total interface trap density (D_{total}), which is calculated from the area under the plot of $D_{it} - (E_c - E_t)$ (inset of Figure 7), has also pronounced that the interface quality improved as a function of PDA temperature, and the obtained D_{total} is in the range of $(3.99–7.34) \times 10^{12}$ cm^{-2}.

Of these investigated samples, it is envisaged that the attainment of the highest positive Q_{eff} as well as the lowest D_{it} and D_{total} has contributed to the sustainability of a sample PDA at 800 °C to withstand a higher electric breakdown field (E_B) and a lower leakage current density (J) than that of the other two samples, which was proven from the acquired J–E characteristics of the investigated samples (Figure 8). As mentioned in a former section, the acquisition of positive trapped charges in the investigated samples is due to the unbonded Ga^{3+} ions, wherein these positive trapped charges have a tendency to capture the injected electrons from the GaN substrate to form a neutral trap. As a result, the injection of electrons needs to be enhanced in order to break the oxide network at a higher electric field. This explains the justification of suppression in the leakage current of a sample PDA at 800 °C through the attainment of the highest density of positive trapped charge than samples PDA at 400 and 600 °C. Besides, it was perceived that ultrathin Al_2O_3 interlayer has assisted in improving the electric breakdown field of Y_2O_3/Al_2O_3/GaN structure subjected to PDA at 800 °C (~12.9 MV/cm), which was higher than that of the Y_2O_3/GaN (~9.7 MV/cm) structure.[14,54] In addition, a comparison based on the safe value of device operation implied that Y_2O_3/Al_2O_3/GaN structure subjected to PDA at 800 °C was able to withstand a higher electric field of approximately 10.2 MV/cm at a 10^{-6} A/cm^2, surpassing that of Y_2O_3/GaN (~6.6 MV/cm)[14,54] and HfO_2/Al_2O_3/GaN (~2.1 MV/cm)[9] structures at a 10^{-6} A/cm^2. Another possible factor contributing to the attainment of the best J–E characteristic by a sample PDA at 800 °C is due to the attainment of the smallest hysteresis (Figure 7). This denotes that the amount of slow traps present in this sample is the lowest when compared with samples PDA at 400 and 600 °C. Slow traps are termed as the trapping and detrapping of charges when the gate bias induced on the gate stack is swept bidirectionally from −8 to +4 V (Figure 7).[29] It is believed that a sample PDA at 800 °C consisted of more donor traps than samples PDA at 400 and 600 °C, wherein these donor traps are initially filled with electrons and electrically neutral. As a result, the tendency of capturing electrons injected from the GaN substrate during forward-bias is reduced and fewer electrons are being released during reverse-bias. Hence, a sample PDA at 800 °C consisted of the lowest slow trap density. Slow trap density (STD) is being calculated using eq 6 to support the estimation of slow traps from the hysteresis of the C–V curves:[29]

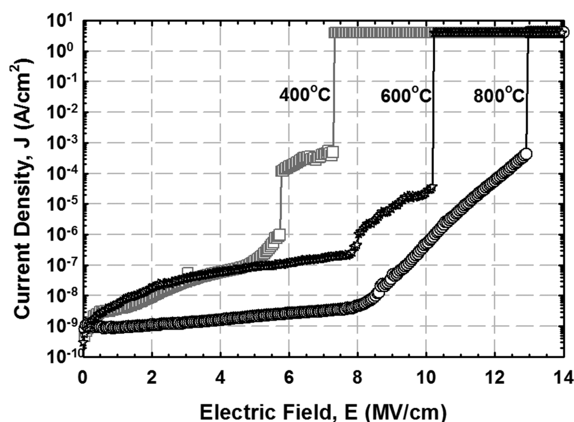

Figure 8. Current density–electric field (J–E) characteristics of Al//Y_2O_3/Al_2O_3/GaN-based MOS capacitors subjected to different PDA temperatures.

$$\text{STD} = \frac{\Delta V C_{ox}}{qA} \quad (6)$$

where ΔV is the difference between forward- and reverse-bias flatband voltage. The calculated value of STD is in the range of $(0.57–2.25) \times 10^{12}$ cm^{-2} for the investigated samples, in which an increment in PDA temperature has contributed to the reduction of STD. The calculated STD is agreement with the trend estimated from hysteresis.

3. CONCLUSIONS

The incorporation of α-Al_2O_3 as an interlayer at the Y_2O_3/GaN interface in Y_2O_3/Al_2O_3/GaN structures PDA from 400 to 800 °C has successfully suppressed the formation of thick interfacial layer. This phenomenon has been described, discussed, and associated with the potential of α-Al_2O_3 as an oxygen interstitial former, which favored the capturing of oxygen species diffused from the Y_2O_3 layer. Occurrence of these would assist in slowing down the oxygen diffusion from the α-Al_2O_3 interlayer to the GaN surface for oxidation to happen. Concurrently, decomposition of GaN substrate occurred and the resulting gaseous Ga^{3+} and N^{3-} would diffuse outward. While diffusing outward, these Ga^{3+} and N^{3-} have been used for charge compensation in the α-Al_2O_3 interlayer with excess N^{3-} ions diffusing further outward to the Y_2O_3 layer. Therefore, α-Al_2O_3 has been described to serve as a layer in the Y_2O_3/Al_2O_3/GaN structure for the accumulation of Ga^{3+} and N^{3-}. The accumulation of Ga^{3+} in the α-Al_2O_3 interlayer has been identified as a contributor leading to the attainment of overall positive charge in the Y_2O_3/Al_2O_3/GaN structure PDA from 400 to 800 °C. Besides, it was determined that the formation of more liquid Ga^{3+} than gaseous Ga^{3+} at lower PDA temperature has triggered the degradation in interface quality, which was supported by the calculated interface trap density (D_{it}) and total interface trap density (D_{total}). In conclusion, a sample PDA at 800 °C is able to sustain the highest breakdown field due to the acquisition of the highest positive effective oxide charge, D_{it}, D_{total}, and slow trap density.

4. EXPERIMENTAL SECTION

First, commercially purchased Si-doped (n-type) GaN epitaxial layers with thickness of 7 μm and doping concentration of 1 to 9 × 10^{18} cm^{-3} grown on sapphire substrates were diced into smaller pieces. Prior to the deposition of Y_2O_3 (~60 nm) and Al_2O_3 (~6 nm) films using RF-magnetron sputtering (HVV AUTO 500), the samples were subjected to RCA (Radio Corporation of America) cleaning. After the cleaning process, these samples were attached to a rotating substrate

holder inside the machine. A high purity argon gas (99.999%) flowing through a gas flow controller was used to purge the chamber, and the base pressure of the system was 1×10^{-6} mbar. Before the commencement of the sputtering process, the surface of the Y_2O_3 and Al_2O_3 targets was cleaned by continuous plasma. During the sputtering process, the chamber pressure was maintained at approximately 2.3×10^{-2} mbar and the argon gas flow rate was configured at 19.3 cm^3 min^{-1}. Sputtering power of 220 and 160 W was used for deposition of Y_2O_3 and Al_2O_3, respectively. The film thickness and sputtering rate was controlled using a quartz crystal monitor (SQM-160). After the deposition, the samples were postdeposition annealed (PDA) in a horizontal tube furnace at 400 to 800 °C in oxygen ambient for 30 min with a heating rate of 10 °C/min. In order to fabricate metal-oxide-semiconductor (MOS) test structures, the Y_2O_3/Al_2O_3 gate stack was selectively etched using HF/H_2O (1:1) solution. After the etching process, a blanket of aluminum (Al) was evaporated on the Y_2O_3/Al_2O_3 gate stack using a thermal evaporator (AUTO 306). Finally, an array of Al gate electrode (area = 2.5×10^{-3} cm^2) was defined using a photolithography process to produce Al/Y_2O_3/Al_2O_3/GaN MOS-capacitors.

X-ray diffraction [(XRD); P8 Advan-Bruker] was used to investigate the phase and orientations of Y_2O_3 and Al_2O_3 in a scan range of 2θ = 25−80° using a step time of 71.59998 ms and a step size of 0.034222°. The Cu Kα radiation (λ = 1.5406 Å) was run under a voltage of 40 kV and a current of 40 mA. In order to obtain the chemical compositional and depth profile of the investigated samples, X-ray photoelectron spectroscopy (XPS) was performed using Kratos Axis Nova equipped with a monochromatic Al Kα X-ray source ($h\nu$ = 1486.69 eV). A spectrometer operating at 160 W and a takeoff angle of 0° with respect to normal surface was utilized. A depth profiling analysis was carried out on an analysis area of 300 × 700 μm^2, and a 4 kV Ar ion etching was utilized. A combination of wide and narrow scans has been used to acquire the chemical compositions of the films. Initially, a wide scan was performed at a low pass-energy of 160 eV for 2 min to determine the elemental chemical states. The core-level spectra of Y 3d, Ga 2p, Al 2p, O 1s, and N 1s had been detected. A pass-energy of 40 eV for 2 min was utilized to perform a narrow scan through the binding-energy range of interest. Linear background and surface charge were corrected prior to the spectra deconvolution and analysis using CasaXPS software (version 2.3.15). All of the spectra were calibrated against the C 1s peak (284.6 eV) of adventitious carbon to compensate the charging effect of the XPS spectra. Focus ion beam was used in the preparation of energy filtered transmission electron microscopy (EFTEM) and high resolution (HR) TEM specimens. EFTEM (Zeiss Libra 200) was used to determine the cross-sectional images of samples PDA at 400 and 800 °C while HRTEM (FEI Tecnai TF-20) was employed for a sample PDA at 600 °C. The average total oxide thickness in the range of 26.4 to 29.6 nm has been determined for PDA samples from 20 different locations (Figure 1). Electron energy loss spectroscopy (EELS) line scan was obtained in scanning TEM (STEM) mode using a nominal 1 nm electron beam, and a Gatan Enfina DigiPEELS spectrometer was used. Semiconductor parameter analyzer (Agilent 4156C) and a parameter analyzer (Keithley 4200-SCS) were used to measure the current−voltage and high frequency capacitance−voltage (100 kHz) characteristics, respectively, of the investigated MOS test structures.

AUTHOR INFORMATION

Corresponding Author

*E-mail: srcheong@usm.my. Tel: +604-5995259. Fax: +604-5941011.

Notes

The authors declare no competing financial interest.

ACKNOWLEDGMENTS

The authors acknowledge Universiti Sains Malaysia, The USM Research University−Postgraduate Research Grant Scheme (8044041), and The Universiti Sains Malaysia Vice Chancellor's Award for their financial support.

REFERENCES

(1) Chang, Y. C.; Chiu, H. C.; Lee, Y. J.; Huang, M. L.; Lee, K. Y.; Hong, M.; Chiu, Y. N.; Kwo, J.; Wang, Y. H. Structural and Electrical Characteristics of Atomic Layer Deposited High k HfO_2 on GaN. *Appl. Phys. Lett.* **2007**, *90*, 232904-1−232904-3.

(2) Wu, Y. Q.; Shen, T.; Ye, P. D.; Wilk, G. D. Photo-Assisted Capacitance-Voltage Characterization of High-Quality Atomic-Layer-Deposited Al_2O_3/GaN Metal-Oxide-Semiconductor Structures. *Appl. Phys. Lett.* **2007**, *90*, 143504-1−143504-3.

(3) Quah, H. J.; Cheong, K. Y. Surface Passivation of Gallium Nitride by Ultrathin RF-Magnetron Sputtered Al_2O_3 Gate. *ACS Appl. Mater. Interfaces* **2013**, *5*, 6860−6863.

(4) Reddy, V. R.; Reddy, M. S. P.; Lakshmi, B. P.; Kumar, A. A. Electrical Characterization of Au/n-GaN Metal-Semiconductor and Au/SiO_2/n-GaN Metal-Insulator-Semiconductor Structures. *J. Alloys Compd.* **2011**, *509*, 8001−8007.

(5) Lee, M.; Ho, C.; Zeng, J. Electrical Properties of Liquid Phase Deposited SiO_2 on Photochemical Treated GaN. *Electrochem. Solid-State Lett.* **2008**, *11*, D9−D12.

(6) Chang, S. J.; Wang, C. K.; Su, Y. K.; Chang, C. S.; Lin, T. K.; Ko, T. K.; Liu, H. L.; GaN, M. I. S. Capacitors with Photo-CVD SiN_xO_y Insulating Layers. *J. Electrochem. Soc.* **2005**, *152*, G423−G426.

(7) Toyoda, S.; Shinohara, T.; Kumigashira, H.; Oshima, M.; Kato, Y. Significant Increase in Conduction Band Discontinuity due to Solid Phase Epitaxy of Al_2O_3 Gate Insulator Films on GaN Semiconductor. *Appl. Phys. Lett.* **2012**, *101*, 231607-1−231607-4.

(8) Hung, T. H.; Krishnamoorthy, S.; Esposto, M.; Nath, D. N.; Park, P. S.; Rajan, S. Interface Charge Engineering at Atomic Layer Deposited Dielectric/III-Nitride Interfaces. *Appl. Phys. Lett.* **2013**, *102*, 072105-1−072105-4.

(9) Chang, Y. C.; Huang, M. L.; Chang, Y. H.; Lee, Y. J.; Chiu, H. C.; Kwo, J.; Hong, M. Atomic-Layer-Deposited Al_2O_3 and HfO_2 on GaN: A Comparative Study on Interfaces and Electrical Characteristics. *Microelectron. Eng.* **2011**, *88*, 1207−1210.

(10) Liu, C.; Chor, E. F.; Tan, L. S.; Dong, Y. Structural and Electrical Characteristics of the Pulsed-Laser-Deposition-Grown Sc_2O_3/GaN Heterostructure. *Appl. Phys. Lett.* **2006**, *88*, 222113-1−222113-3.

(11) Chang, Y. C.; Lee, Y. J.; Chiu, Y. N.; Lin, T. D.; Wu, S. Y.; Chiu, H. C.; Kwo, J.; Wang, Y. H.; Hong, M. MBE Grown High k Dielectrics $Ga_2O_3(Gd_2O_3)$ on GaN. *J. Cryst. Growth* **2007**, *301*, 390−393.

(12) Chang, W. H.; Lee, C. H.; Chang, P.; Chang, Y. C.; Lee, Y. J.; Kwo, J.; Tsai, C. C.; Hong, J. M.; Hsu, C. H.; Hong, M. High k Dielectric Single-Crystal Monoclinic Gd_2O_3 on GaN with Excellent Thermal, Structural, and Electrical Properties. *J. Cryst. Growth* **2009**, *311*, 2183−2186.

(13) Quah, H. J.; Cheong, K. Y. Current Conduction Mechanisms in RF-Magnetron Sputtered Y_2O_3 Gate on GaN Under Different Post-Deposition Annealing Ambient. *Sci. Adv. Mater.* **2013**, *5*, 1816−1827.

(14) Quah, H. J.; Cheong, K. Y. Effects of Post-Deposition Annealing Ambient on Chemical, Structural, and Electrical Properties of RF Magnetron Sputtered Y_2O_3 Gate on Gallium Nitride. *J. Alloys Compd.* **2013**, *575*, 382−392.

(15) Nakano, Y.; Jimbo, T. Interface Properties of Thermally Oxidized n-GaN Metal-Oxide-Semiconductor Capacitors. *Appl. Phys. Lett.* **2003**, *82*, 218−220.

(16) Zhou, Y.; Ahyi, C.; Smith, T. I.; Bozack, M.; Tin, C.; Williams, J.; Park, M.; Cheng, A.; Park, J.; Kim, D.; Wang, D.; Preble, E. A.; Hanser, A.; Evans, K. Formation, Etching and Electrical Characterization of a Thermally Grown Gallium Oxide on the Ga-Face of a Bulk GaN Substrate. *Solid-State Electron.* **2008**, *52*, 756−764.

(17) Hsiao, C. Y.; Shih, C. F.; Chien, C. H.; Huang, C. L. Textured Magnesium Titanate as Gate Oxide for GaN-Based Metal-Oxide-Semiconductor Capacitor. *J. Am. Ceram. Soc.* **2011**, *94*, 1005−1007.

(18) Tu, L. W.; Kuo, W. C.; Lee, K. H.; Tsao, P. H.; Lai, C. M.; Chu, A. K.; Sheu, J. K. High-Dielectric Constant Ta_2O_5/n-GaN Metal-

Oxide-Semiconductor Structure. *Appl. Phys. Lett.* **2000**, *77*, 3788−3790.
(19) Polyakov, A. Y.; Smirnov, N. B.; Gila, B. P.; Hlad, M.; Gerger, A. P.; Abernathy, C. R.; Pearton, S. J. Studies of Interface States in Sc_2O_3/GaN, MgO/GaN, and MgScO/GaN Structures. *J. Electrochem. Soc.* **2007**, *154*, H115−H118.
(20) Quah, H. J.; Cheong, K. Y.; Hassan, Z.; Lockman, Z. Effects of N_2O Postdeposition Annealing on Metal-Organic Decomposed CeO_2 Gate Oxide Spin-Coated on GaN Substrate. *J. Electrochem. Soc.* **2011**, *158*, H423−H432.
(21) Quah, H. J.; Cheong, K. Y.; Hassan, Z.; Lockman, Z. Effect of Postdeposition Annealing in Oxygen Ambient on Gallium-Nitride-Based MOS Capacitors with Cerium Oxide Gate. *IEEE Trans. Electron Devices* **2011**, *58*, 122−131.
(22) Liu, X.; Chin, H. C.; Tan, L. S.; Yeo, Y. C. High-Permittivity Dielectric Stack on Gallium Nitride Formed by Silane Surface Passivation and Metal-Organic Chemical Vapor Deposition. *IEEE Electron Device Lett.* **2010**, *31*, 8−10.
(23) Korzenski, M. B.; Lecoeur, Ph.; Mercey, B.; Chippaux, D.; Ravaeu, B. PLD-Grown Y_2O_3 Thin Films from Y Metal: An Advantageous Alternative to Films Deposited from Yttria. *Chem. Mater.* **2000**, *12*, 3139−3150.
(24) Fidancev, E. A.; Holsa, J.; Lastusaari, M. Crystal Field Strength in C-Type Cubic Rare Earth Oxides. *J. Alloys Compd.* **2002**, *341*, 82−86.
(25) Som, S.; Sharma, S. K. Eu^{3+}/Tb^{3+}-Codoped Y_2O_3 Nanophosphors: Rietveld Refinement, Bandgap and Photoluminescence Optimization. *J. Phys. D: Appl. Phys.* **2012**, *45*, 415102-1−415102-11.
(26) Sougleridis, V. I.; Constantoudis, V.; Alexe, M.; Scholz, R.; Vellianitis, G.; Dimoulas, A. Effects on Surface Morphology of Epitaxial Y_2O_3 Layers on Si (001) After Post-Growth Annealing. *Thin Solid Films* **2004**, *468*, 303−309.
(27) Travlos, A.; Boukos, N.; Apostolopoulos, G.; Dimoulas, A. Oxygen Vacancy Ordering in Epitaxial Layers of Yttrium Oxide on Si (001). *Appl. Phys. Lett.* **2003**, *82*, 4053−4055.
(28) Rastogi, A. C.; Sharma, R. N. Interfacial Charge Trapping in Extrinsic Y_2O_3/SiO_2 Bilayer Gate Dielectric Based MIS Devices on Si(100). *Semicond. Sci. Technol.* **2001**, *16*, 641−650.
(29) Quah, H. J.; Cheong, K. Y. Study on Gallium Nitride-Based Metal-Oxide-Semiconductor Capacitors with RF Magnetron Sputtered Y_2O_3 Gate. *IEEE Trans. Electron Devices* **2012**, *59*, 3009−3016.
(30) Hori, Y.; Mizue, C.; Hashizume, T. Process Conditions for Improvement of Electrical Properties of Al_2O_3/n-GaN Structures Prepared by Atomic Layer Deposition. *Jpn. J. Appl. Phys.* **2010**, *49*, 080201-1−080201-3.
(31) Robertson, J.; Falabretti, B. Band Offsets of High K Gate Oxides on III-V Semiconductors. *J. Appl. Phys.* **2006**, *100*, 014111-1−014111-8.
(32) Yang, M. Y.; Kamiya, K.; Shiraishi, K. Interstitial Oxygen Induced Fermi Level Pinning in the Al_2O_3-Based High-k MISFET with Heavy-Doped n-Type Poly-Si Gates. *AIP Adv.* **2013**, *3*, 102113-1−102113-7.
(33) Gamallo, P.; Sayos, R. A Density Functional Theory Study of Atomic Oxygen and Nitrogen Adsorption Over α-Alumina (0001). *Phys. Chem. Chem. Phys.* **2007**, *9*, 5112−5120.
(34) Sokol, A. A.; Walsh, A.; Catlow, C. R. A. Oxygen Interstitial Structures in Close-Packed Metal Oxides. *Chem. Phys. Lett.* **2010**, *492*, 44−48.
(35) Koleske, D. D.; Wickenden, A. E.; Henry, R. L.; Culbertson, J. C.; Twigg, M. E. GaN Decomposition in H_2 and N_2 at MOVPE Temperatures and Pressures. *J. Cryst. Growth* **2001**, *223*, 466−483.
(36) Xia, X.; Oldman, R. J.; Catlow, C. R. A. Oxygen Adsorption and Dissociation on Yttria Stabilized Zirconia Surfaces. *J. Mater. Chem.* **2012**, *22*, 8594−8612.
(37) Henderson, M. A.; Epling, W. S.; Perkins, C. L.; Peden, C. H. F. Interaction of Molecular Oxygen with the Vacuum-Annealed TiO_2 (110) Surface: Molecular and Dissociative Channels. *J. Phys. Chem. B* **1999**, *103*, 5328−5337.
(38) Epling, W. S.; Peden, C. H. F.; Henderson, M. A.; Diebold, U. Evidence for Oxygen Adatoms on TiO_2 (110) Resulting from O_2 Dissociation at Vacancy Sites. *Surf. Sci.* **1998**, *412/413*, 333−343.
(39) Anders, K.; Jusza, A.; Baran, M.; Lipinska, L.; Piramidowicz, R. Emission Properties of Polymer Composites Doped with Er^{3+}:Y_2O_3 Nanopowders. *Opt. Mater.* **2012**, *34*, 1964−1968.
(40) Chen, H. T.; Chang, J. G.; Chen, H. L.; Ju, S. P. Identifying the O_2 Diffusion and Reduction Mechanisms on CeO_2 Electrolyte in Solid Oxide Fuel Cells: A DFT + U Study. *J. Comput. Chem.* **2009**, *30*, 2433−2442.
(41) Lim, W. F.; Cheong, K. Y. Structural and Chemical Studies of Metal-Organic Decomposed $La_xCe_yO_z$ Thin Film as a Catalytic Oxide on 4H-SiC as a Function of Postdeposition Annealing Time. *J. Phys. Chem. C* **2013**, *117*, 14014−14024.
(42) Heinmaa, I.; Joon, T.; Kooskora, H.; Pahapill, J.; Subbi, J. Local Structure and Oxygen Ion Dynamics in La Doped Ceria: ^{17}O NMR Study. *Solid State Ionics* **2010**, *181*, 1309−1315.
(43) Liu, L.; Way, X.; Guo, M.; Zhang, M. Kinetics Investigation of Oxygen Storage Capacity in La_2O_3-CeO_2 Solid Solution. *J. Nanosci. Nanotechnol.* **2011**, *11*, 2155−2162.
(44) Zywitzki, O.; Hoetzsch, G.; Fietzke, F.; Goedicke, K. Effect of the Substrate Temperature on the Structure and Properties of Al_2O_3 Layers Reactively Deposited by Pulsed Magnetron Sputtering. *Surf. Coat. Technol.* **1996**, *82*, 169−175.
(45) Wang, P. W.; Hsu, J. C.; Lin, Y. H.; Chen, H. L. Structural Investigation of High-Transmittance Aluminum Oxynitride Films Deposited by Ion Beam Sputtering. *Surf. Interface Anal.* **2011**, *43*, 1089−1094.
(46) Huang, L. H.; Kan, K. C.; Lee, C. T. Analysis of Oxidized p-GaN Films Directly Grown Using Bias-Assisted Photoelectrochemical Method. *J. Electron. Mater.* **2009**, *38*, 529−532.
(47) Lee, C. T.; Chen, H. W.; Hwang, F. T.; Lee, H. Y. Investigation of Ga Oxide Films Directly Grown on n-Type GaN by Photoelectrochemical Oxidation Using He-Cd Laser. *J. Electron. Mater.* **2005**, *34*, 282−286.
(48) Pan, T. M.; Lee, J. D. Physical and Electrical Properties of Yttrium Oxide Gate Dielectrics on Si Substrate with NH_3 Plasma Treatment. *J. Electrochem. Soc.* **2007**, *154*, H698−H703.
(49) Durand, C.; Dubourdieu, C.; Vallee, C.; Loup, V.; Bonvalot, M.; Joubert, O.; Roussel, H.; Renault, O. Microstructure and Electrical Characterizations of Yttrium Oxide and Yttrium Silicate Thin Films Deposited by Pulsed Liquid-Injection Plasma Enhanced Metal-Organic Chemical Vapor Deposition. *J. Appl. Phys.* **2004**, *96*, 1719−1729.
(50) Durand, C.; Dubourdieu, C.; Vallee, C.; Gautier, E.; Ducroquet, F.; Jalabert, D.; Roussel, H.; Bonvalot, M.; Joubert, O. Structural and Electrical Characterizations of Yttrium Oxide Films after Postannealing Treatments. *J. Electrochem. Soc.* **2005**, *152*, F217−F225.
(51) Cruz, W. D. L.; Diaz, J. A.; Mancera, L.; Takeuchi, N.; Soto, G. Yttrium Nitride Thin Films Grown by Reactive Laser Ablation. *J. Phys. Chem. Solids* **2003**, *64*, 2273−2279.
(52) Wang, X. J.; Zhang, L. D.; He, G.; Zhang, J. P.; Liu, M.; Zhu, L. Q. Effects of Postdeposition Annealing on the Structure and Optical Properties of YO_xN_y Films. *J. Appl. Phys.* **2008**, *103*, 064101-1−064101-7.
(53) Schroder, D. K. *Semiconductor Material and Device Characterization*, 2nd ed; Wiley: New York, 1998.
(54) Quah, H. J.; Cheong, K. Y. Effects of Post-Deposition Annealing Ambient on Band Alignment of RF Magnetron Sputtered Y_2O_3 Film on Gallium Nitride. *Nanoscale Res. Lett.* **2013**, *8*, 53-1−53-7.